RESEARCH PAPER

Effects of welding parameters on micro-junction structure and fracture behavior of refill friction stir spot welded joints for 2060 aluminum alloys

Yue Wang [1,2] • Peng Chai [1,2]

Abstract

Due to different filling modes of the material in sleeve-affected zone (SAZ), probe-affected zone (PAZ), and thermo-mechanically affected zone (TMAZ), the micro-junction structure is formed at the bottom of the SAZ of the refill FSSW joint for 3.2-mm-thick 2060 aluminum alloys. The plasticized degree of the filling material and refilling time greatly affect the morphologies of micro-junction structure. Thus, the welding defects such as void with different sizes, kissing bond, and crack are easily formed in the micro-junction structure. Besides, the tensile-shear properties are related to the micro-junction structure and bonding strength of the lap interface. The increase of the plunge depth or rotation speed within a certain range enhances the flow of material in the stir zone and increases the atomic diffusion capacity of the lap interface, which is beneficial to increasing the tensile-shear load. The maximum tensile-shear load was obtained when the rotation speed of 2500 rpm and the plunge depth of 4 mm are used, and the tensile-shear specimen fractures along the bottom of the SAZ. Other fracture paths are also obtained under different welding parameters combinations, first along the lap interface, and second, not only along the lap interface but along the SAZ bottom.

Keywords Refill friction stir spot weld · 2060 aluminum alloys · Micro-junction structure · Welding defect · Fracture behavior

1 Introduction

Element Li as the lightest element is added into aluminum alloys to form the aluminum lithium alloys, which decreases aluminum alloys' density while increases strength and modulus. Furthermore, aluminum lithium alloys have good corrosion resistance and fatigue resistance. Since the development of aluminum lithium alloys, they have been widely used in aerospace [1, 2]. Lap-joined joints are common structural forms in aviation structures. The drilling prior to connection and the weight increment of rivets are not avoided when

riveting is used. The fusion welding technologies have the disadvantages such as porosity, large heat deformation, and coarse microstructure [3, 4]. Refill friction stir spot welding (refill FSSW), invented by HZG (formerly known as GKSS) in 2002, is a solid-state welding technology [5]. This joining process not only does not increase the weight of the structure but also consumes less energy [6].

Castro et al. [7] investigated the effect of welding parameters on mechanical properties of refill FSSW joints for a 1.6-mm-thick 2198-T8 aluminum alloy according to Taguchi method, and results show that rotation speed and plunge depth are responsible for more than 80% of strength variance. A similar result has been reported by Tier et al [8]. Kluz et al. [9] found that tool rotation speed has the greatest impact on the load-carrying capacity of the refill FSSW joint for 7075 aluminum alloys. Defects are the main factors to influence the formation and mechanical properties of joints. Welding defects depending on their location in joints occur at the sleeve-plunger interface, at the lap interface, and in the joint axis [10]. The groove and kissing bonding at the sleeve-plunger interface can be eliminated by setting the end faces of the sleeve and probe lower than the original upper surface
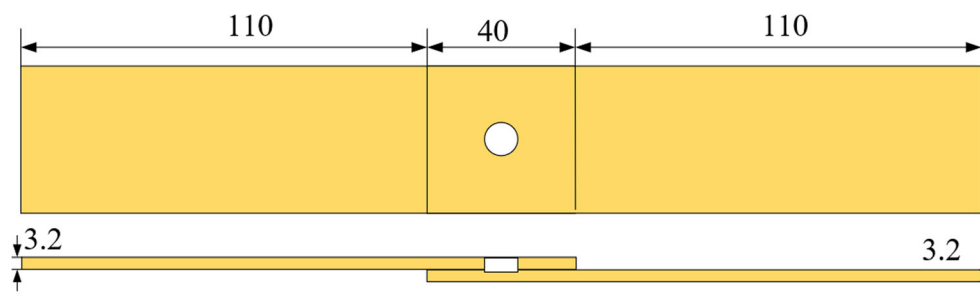

✉ Yue Wang
endlesswy@163.com

1 School of Mechanical Engineering and Automation, Beihang University, Beijing 100083 China

2 Beijing FSW Technology Co., Ltd, AVIC Manufacturing Technology Institute, Beijing 100024 China

Fig. 1 Schematic of the tensile-shear specimen

of the upper sheet at the end of the refilling phase [11]. Hook and bonding ligament at the lap interface are interior features and can be observed in the metallurgical connection area of cross section [12]. However, hook and bonding ligament can be decreased but cannot be eliminated by optimizing welding parameters. When the welding temperature at the bottom sheet is not high enough, a crater is formed in the joint axis [10]. When the welding parameters are improper or the sleeve does not penetrate the interface between the sheets, the welding defects such as crack and void occur [13]. Yue et al. [14] reported that the void in the 2198 aluminum alloy refill FSSW joints is attributed to the insufficient refilling effect induced by material loss. Lowering the plunge depth can eliminate the void [14]. Shen et al. [15, 16] reported that the void is associated with insufficient material flow. Decreasing the rotation speed or increasing the dwell time is beneficial for obtaining defect-free refill FSSW joints [15, 16]. However, the void in the 2198 aluminum alloy refill FSSW joints can be eliminated by increasing the rotation speed [17]. Other scholars explained the void to thermal shrinkage, entrapped air, or some physical–chemical reactions [18]. Void belonging to volumetric defect not only decreases the load-carrying area under external load but also increases the crack initiation points. The most critical phase in controlling fracture toughness is the control of the initiation of voids, because particles provide interfaces that are easy initiation sites for voids [13].

From the published literatures, the welding defects can be easily generated in refill FSSW joints for 2xxx series aluminum alloys under improper welding parameter combinations [1, 12, 13, 17, 18]. These defects including void, crack, and kissing bond usually occur at the bottom of the sleeve-plunging path where the material has complex flow state. Thus, a micro-junction structure with complex material flow is observed at the bottom of the sleeve-plunging path. This study selects the 2060 aluminum alloy widely used in aerospace as the research object. The formation mechanism of the micro-junction structure and effects of welding parameters including rotation speed and plunge depth on micro-junction structure and fracture behavior of refill FSSW joints are investigated.

2 Experimental material and methods

In this study, the 3.2-mm-thick 2060 aluminum alloys with the length of 150 mm and the width of 40 mm were used to obtain the refill FSSW joint. Prior to welding, the upper and lower surfaces of sheets were polished to wipe off the oxidations. Two sheets were overlapped with $40 \times 40 \text{mm}^2$ and were joined in the center of the overlapped area, as shown in Fig. 1.

Figure 2 shows the refill FSSW robot equipment. This equipment consists of the robot body and welding head. The

Fig. 2 Welding equipment
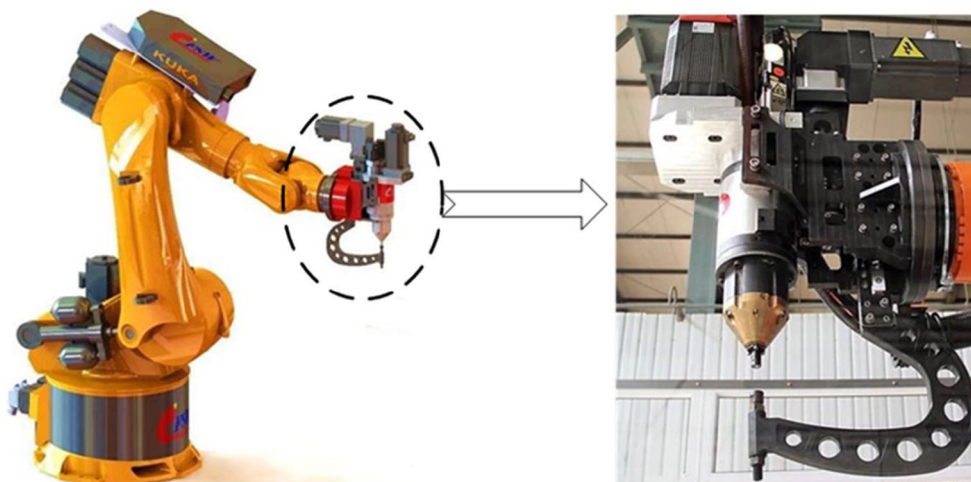
Table 1 Refill FSSW welding parameters for the 2060 aluminum alloy

Number of parameters	Rotation speed/r rpm	Plunge depth/p mm
1-1	2500	3.4
1-2		3.6
1-3		3.8
1-4		4.0
2-1	2000	4.0
2-2	2200	
2-3	2400	
2-4	2600	

welding head, which was designed and manufactured by Beijing FSW Technology Co., Ltd., can reach a maximum welding thickness of 4 mm. The outer diameters of the probe, sleeve, and clamping ring are 6, 9, and 18 mm, respectively. After the welding tool components were assembled to the welding machine, radial run-out of the probe, and the sleeve needed to be measured to avoid friction among components, and the tolerance should be in the range of 0~0.05 mm. However, the axial and radial tolerances of the clamping ring are not measured during the welding process because the clamping ring is not movable axially and radially relative to the welding head, and it only plays the role of fixing welding sheets and preventing material overflow.

Table 1 shows the welding parameters for refill FSSW experiments. The numbers of 1-1 to 1-4 represent the joints at the plunge depth of 3.4–4 mm and the fixed rotation speed of 2500 rpm. The numbers of the 2-1 to 2-4 represent the joints at the rotation speed of 2000–2600 rpm and the fixed plunge depth of 4 mm. The plunge speed and refill speed were both fixed at 50 mm/min.

The refill FSSW joints were cut along the center of the welding spot to obtain the cross-section specimens. Three cross sections of welds under each welding parameter were observed to ensure the accuracy and stability of the results. Each cross-section specimen was burnished, polished, and etched using Keller's reagent. The cross section and

microstructures were observed using an optical microscope (OM). The tensile-shear test was performed three times for each welding parameter in accordance with the standard of ISO 6892-1-2009 "Metallic materials-Tensile testing-Part 1: Method of test at room temperature, and tensile-shear specimens." Furthermore, the fracture surfaces were observed using a scanning electron microscope (SEM).

3 Experimental results

3.1 Structure of refill FSSW joints

During the refill FSSW process, due to the cylindrical welding tool, the cross section of the refill FSSW joint presents a "U" shape (Fig. 3). Due to different thermal cycle and mechanical action, the refill FSSW joint can be also divided into base material (BM), heat-affected zone (HAZ), thermo-mechanically affected zone (TMAZ), and stir zone (SZ). For the refill FSSW of shoulder plunge mode, although the probe dose not plunge into the material at all during the welding process, the majority of the published literatures divide the SZ into probe-affected zone (PAZ) and sleeve-affected zone (SAZ) [13, 14, 17, 19].

Figure 4 shows the cross sections and magnified views of refill FSSW joints under different plunge depths. The regions of the HAZ, TMAZ, and SZ are observed in all the refill FSSW joints. The morphologies of the SZ are identified when the plunge depth is lower than and equal to 4 mm. Note that the height variation of the PAZ under the plunge depth of 3.4–3.6 mm is notable (Fig. 4a–b), and the height values of the PAZ are 1.790 mm and 2.857 mm corresponding to the plunge depths of 3.4 mm and 3.6 mm, respectively. When the plunge depth increases to 3.8 mm, no obvious change in height of the PAZ is observed, and the value is 2.861 mm. No change in the PAZ height is observed as the plunge depth is up to 4 mm.

When the sleeve plunge into the sheet, the material below the probe occurs blanking along the sleeve-plunger path, and thus the material which is in contact with the sleeve occurs severe plastic deformation. The variation of the PAZ height is mainly related to the thermal deformation volume of this part
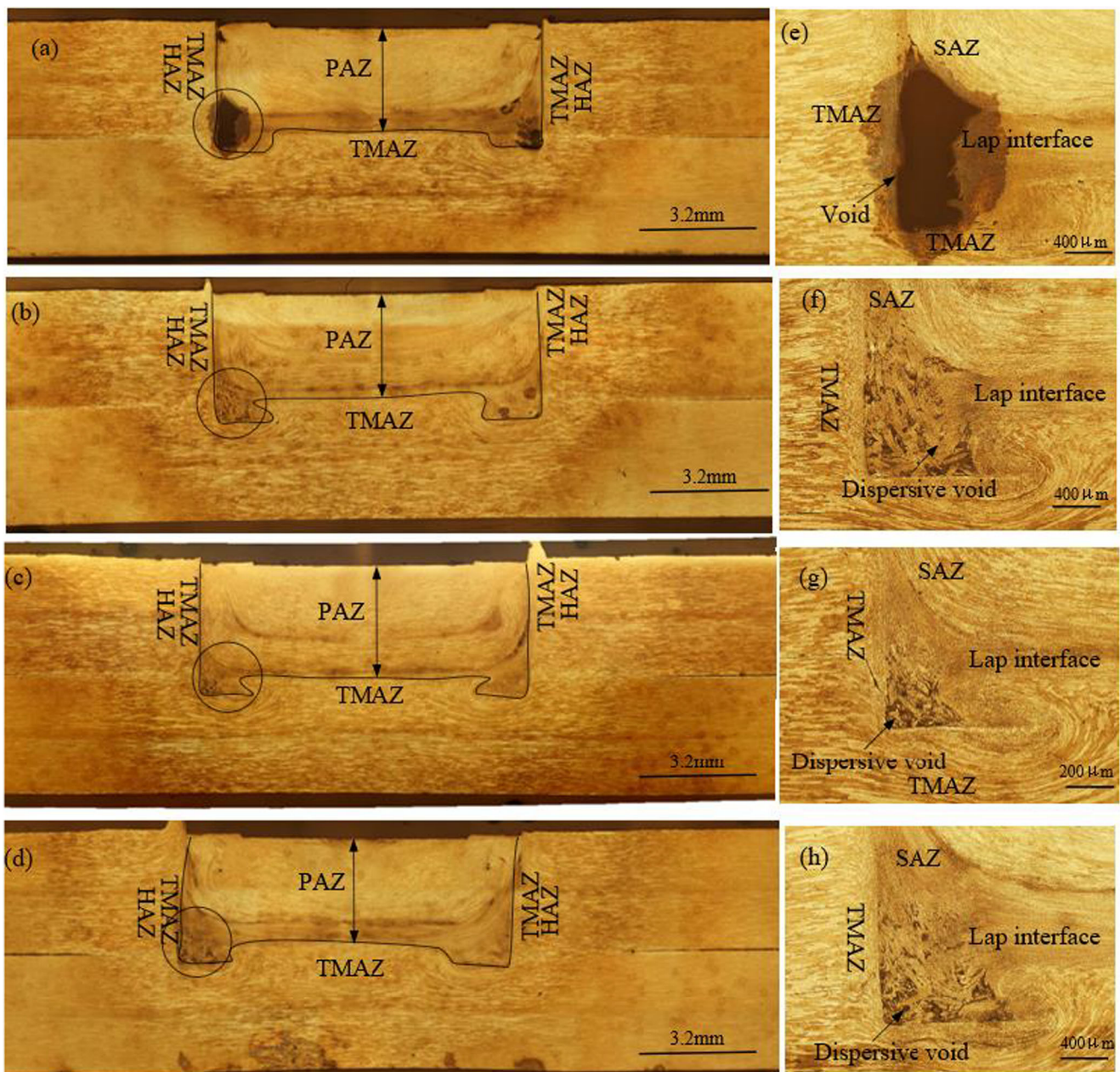
Fig. 3 Different zones of refill FSSW joint
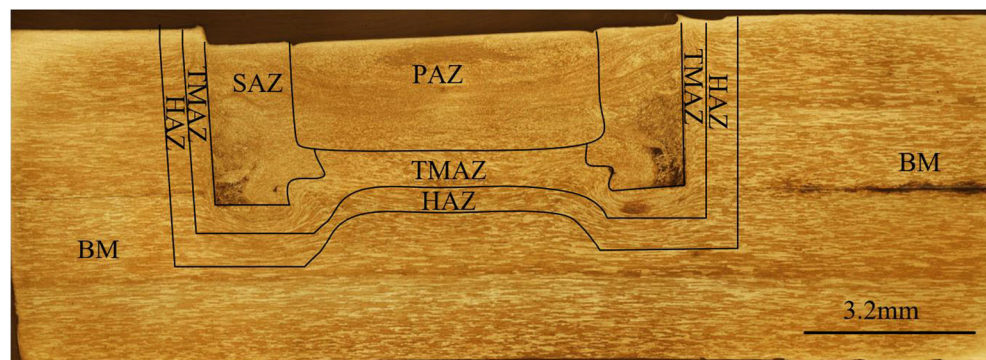
Fig. 4 Cross-sectional structures of refill FSSW joints at different plunge depths: **a, e** 3.4 mm; **b, f** 3.6 mm; **c, g** 3.8 mm; **d, h** 4 mm

of the material under different plunge depths. Zhao et al. [20] pointed out that the welding time and peak temperature of the SZ increase as the plunge depth increases from 2 to 3.5 mm for the 2-mm-thick Al-Zn-Mg-Cu alloy. Similarly, when the plunge depth increases from 3.4 to 3.6 mm, the welding time and heat generation increase. Thus, the volume of the deformed material increases, which increases the height of the

PAZ with increasing plunge depth from 3.4 to 3.6 mm. Zhao et al. [20] also pointed out that the peak temperature of the 2-mm-thick Al-Zn-Mg-Cu alloy refill FSSW joints exceeded the solid-state temperature at rotation speed of 2000 rpm, and the peak temperature of the SZ did not increase as the rotation speed increased to 2500 rpm. Based on these results, it can be inferred that when the rotation speed increases to 3.8 mm and

Fig. 5 Cross-sectional structures of refill FSSW joints at different rotation speeds: **a**, **e** 2000 rpm; **b**, **f** 2200 rpm; **c**, **g** 2400 rpm; **d**, **h** 2600 rpm

4 mm, the non-change of the PAZ height may be related to the non-change of the material for thermal deformation, which in turn is related to the constant peak temperature. Thus, when the plunge depth continues to increase, although the welding time increases, the temperature variation of the material in contact with the shoulder is limited. Therefore, when the plunge depth reaches 3.8 mm and 4 mm, the PAZ height is almost no change. Furthermore, the SZ of the joint under the plunge depth of 4 mm includes two different morphologies. One is elongated grains similarity to the BM, and the other surrounds the elongated grains, as shown in Fig. 4d.

Additionally, the slight surface indentation can be observed in all the joints. It is formed by setting the end faces of the sleeve

and the probe lower than the original upper surface of the upper sheet at the end of the refilling phase [11]. The welding defects can be visually observed not only in the top surface, but also at the bottom of the SZ. At the bottom of the SAZ, defect morphologies inside the joints under different plunge depths are different, and even at the same plunge depth they are also discrepant. In other words, the morphologies of the defects at the bottom of the SAZ are asymmetrical (Fig. 4). Figure 4e–h shows the magnified views of the region at the bottom of the SAZ. At low plunge depth of 3.4 mm, the region with large-area dispersed void can be seen (Fig. 4e). With the increase of the plunge depth, much more material is squeezed into the space at the bottom of the sleeve, and the void in small size is observed (Fig. 4f). The size and

quantity of the void gradually decreases when the plunge depth continues to increase to 3.8 mm and 4 mm (Fig. 4g and h).

Under the plunge depth of 4 mm, with the increase of rotation speed from 2000 to 2400 rpm, the PAZ height has no obvious change (Fig. 5a–c). When the rotation speed increases to 2600 rpm, the SZ height is slightly reduced (Fig. 5d). Furthermore, the defect at the bottom of the SAZ are still asymmetric. The larger defect at the bottom of the SAZ is magnified in Fig. 5e–h. At low rotation speed of 2000 rpm, the void is rather large (Fig. 5e). With the increase of the rotation speed, the large void is refilled, but some dispersed void occurs (Fig. 5f–g). When the rotation speed increases from 2200 to 2400 rpm, the area of the dispersed void is reduced (Fig. 5f–g). When the rotation speed gradually reaches 2500 rpm, only several small voids can be observed (Fig. 4h). However, the dispersed void occurs again as the rotation speed increases to 2600 rpm (Fig. 5h).

Moreover, the grain morphologies of the region at the bottom of the SAZ at different rotation speeds in this study can be divided into two different types including grains at the lap interface and elongated grains in the SAZ, as marked in Fig. 5e–h.

## 3.2 Microstructural characteristics of refill FSSW joints

Figure 6 shows the microstructures of refill FSSW joints at the rotation speed of 2600 rpm and the plunge depth of 4 mm. The BM is characterized by elongated grains (Fig. 6a). Only undergone thermal cycle, the grains in the HAZ are coarsened (Fig. 6b). Due to the moderate thermal cycle and mechanical stir, the microstructure in the TMAZ is deformed (Fig. 6c). The microstructure in the SZ is totally different from other zones, and it is characterized by small equiaxed grains due to dynamic recrystallization (Fig. 6d).

Figure 7 shows morphologies at the lap interfaces of joints under different plunge depths and the given rotation speed of 2500 rpm. When the plunge depth is 3.4 mm, the unconnected defect is obvious at the lap interface (Fig. 7a). The top region of the defect is characterized by deformed grains similar as grains in the BM, while these grains are squeezed and elongated (Fig. 7a). Thus, the deformed grains are regarded as TMAZ. Above the TMAZ, the refined equiaxed grains can be observed. The unconnected defect is disappeared with the increase of the plunge depth. However, the bonding line occurs at the lap interface (Fig. 7–d). From the magnified views, the TMAZ above the bonding line disappears, and this region consists of equiaxed grains in some certain directions. The grains below the bonding line are similar that of the BM.

Figure 8 shows microstructure morphologies at the lap interfaces of joints at different rotation speeds and the given plunge depth of 4 mm. The microstructure morphologies at the lap interfaces of joints under the plunge depth of 4 mm are different from those when the plunge depth is below 4 mm (Fig. 7a–c). The microstructure morphologies at the lap interface are layered along the sheet thickness, and the equiaxed grains are sandwiched between flattened strip grains. The fine equiaxed grains distribute at the bonding interface, and the thickness of the equiaxed grains varies from the rotation speed. The flattened strip grains which

Fig. 6 Microstructures of the refill FSSW joint at the rotation speed of 2600 rpm and the plunge depth of 4 mm: **a** BM, **b** HAZ, **c** TMAZ, and **d** SZ
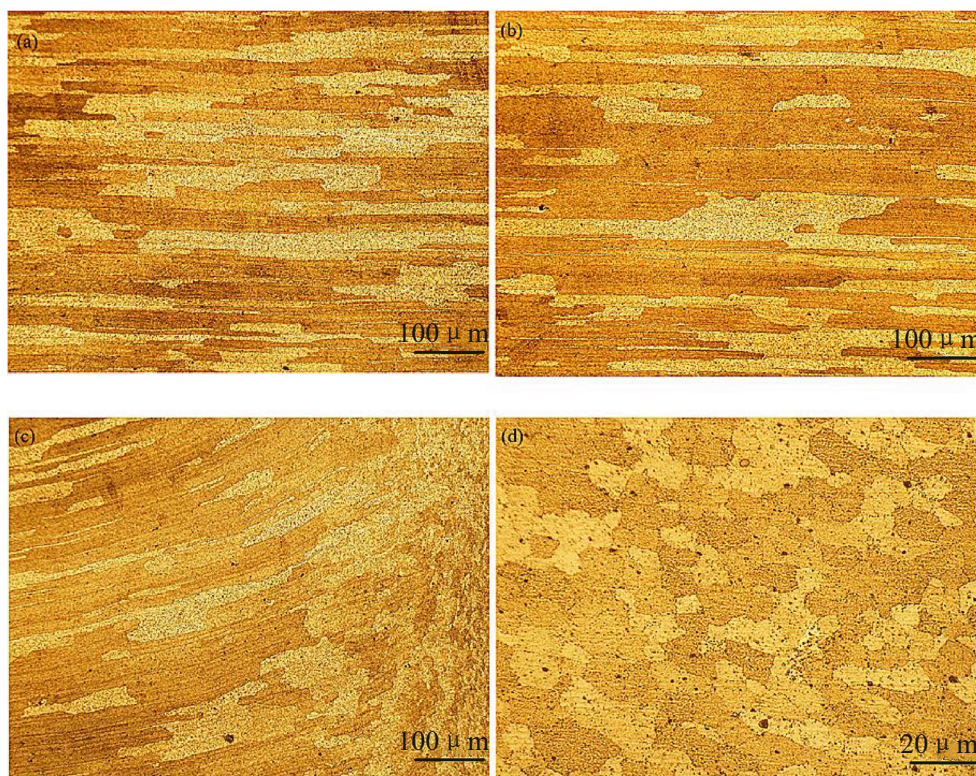
Fig. 7 Lap interfaces of refill FSSW joints under different plunge depths: **a** 3.4 mm, **b** 3.6 mm, **c** 3.8 mm, and **d** 4 mm
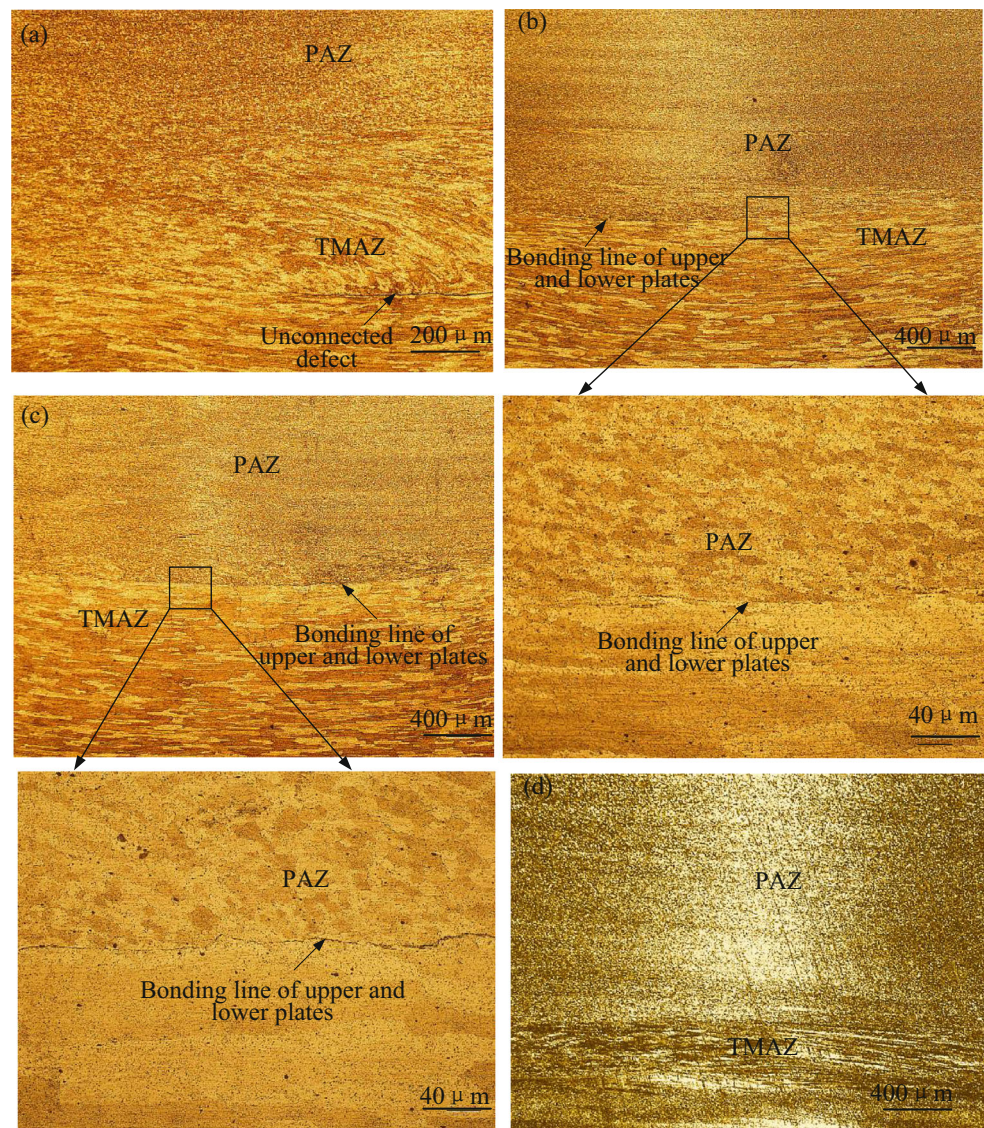
are called TMAZ are located at the upper and lower regions of this equiaxed grains. The void occurs in the bonding interface when the rotation speeds are 2000 rpm and 2600 rpm (Fig. 8a and d). With the decreased distance from the top surface, the effect of stirring by the rotation probe increases, and the microstructure next to the TMAZ exhibits equiaxed grains.

To sum up, welding parameters have an important influence on the microstructure at lap interface. Different microstructures further influence the tensile-shear load and fracture behavior of the joint in turn.

### 3.3 Tensile-shear load and fracture behavior of refill FSSW joints

Figure 9 shows the effect of welding parameters on mean tensile-shear load of refill FSSW joints for the 2060 aluminum alloy. Figure 9a shows that the mean tensile-shear load of the

joint at the fixed rotation speed of 2500 rpm continuously increases with the increase of the plunge depth. Due to the limitation of the welding capacity of the welding equipment, the maximum value of the plunge depth is up to 4 mm. Under this plunge depth, the mean tensile-shear load of the joint reaches the largest at fixed rotation speed of 2500 rpm (Fig. 9a), and then the effect of rotation speed on the tensile-shear load is analyzed at the plunge depth of 4 mm (Fig. 9b). The mean tensile-shear load exhibits an overall rise-drop trend as the rotation speed increases from 2000 to 2600 rpm. The mean tensile-shear load is up to the peak value of 10.64 kN at the rotation speed of 2500 rpm. When the rotation speed is further increased to 2600 rpm, the tensile-shear load reduces rapidly.

Figure 10 shows the typical load-displacement curves of refill FSSW joints under different welding parameter combinations. The tensile-shear load and fracture displacement reach the maximum at the plunge depth of 4 mm and the

Fig. 8 Lap interfaces of refill FSSW joints at different rotation speeds: **a** 2000 rpm, **b** 2200 rpm, **c** 2400 rpm, and **d** 2600 rpm
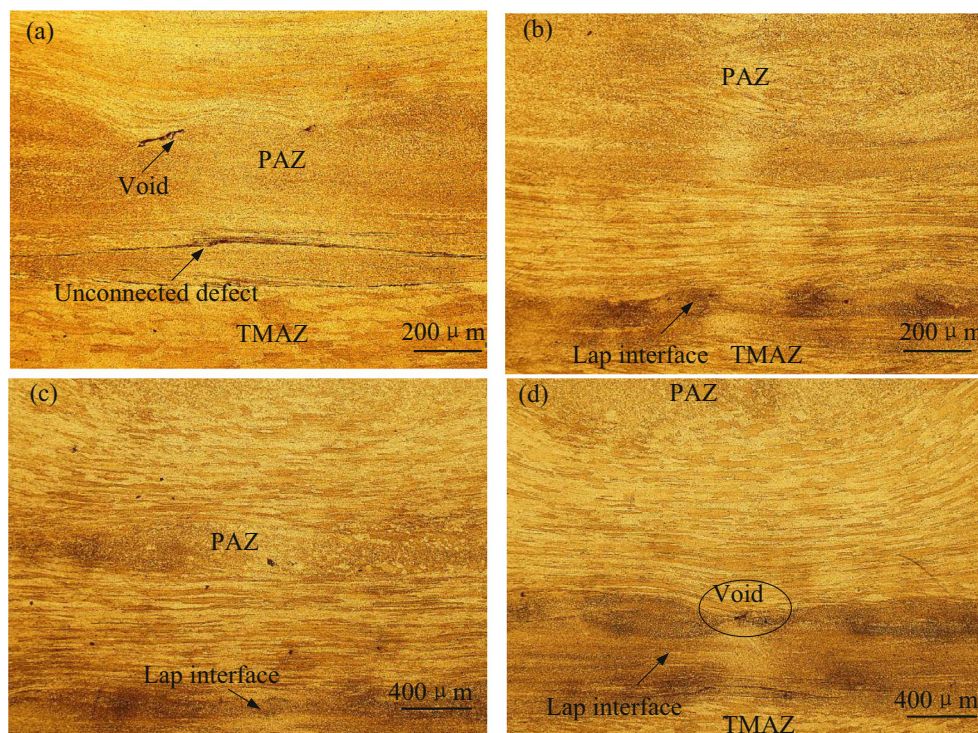
rotation speed of 2500 rpm (Fig. 10a). Furthermore, the load-displacement curves in Fig. 10a are relatively smooth. However, the load-displacement curves under different rotation speeds fluctuate, and there exists obvious the phenomenon of "pop-in" (Fig. 10b). The "pop-in" is related to the decrease of the load carrying area, and the initiation and propagation of cracks.

Figure 11 shows the fracture paths of tensile-shear specimens under different welding parameter combinations. Note that all the tensile-shear specimens apparently have the similar fracture mode which is presented by the separation of the upper and lower sheets. However, different fracture paths are observed under different welding parameter combinations.

When the plunge depth is lower than 4 mm, the tensile-shear specimens at the fixed rotation speed of 2500 rpm fractured along the lap interface (Fig. 11a–c). As the plunge depth increases to 4 mm, fracture paths of tensile-shear specimens at different rotation speeds are complicate. The tensile-shear specimens at low rotation speed of 2000 rpm still fracture along the lap interface (Fig. 11e). When the rotation speed increases to 2200 rpm, a part of the fracture path is located at the bottom of the SZ, and the others are located at the lap interface (Fig. 11f). The fracture surface of the junction between the lap interface and the SZ bottom presents a blunt wedge pattern at an angle of about 45° to the tensile-shear axis (Fig. 11f). As the rotation speed increases to 2400 rpm and
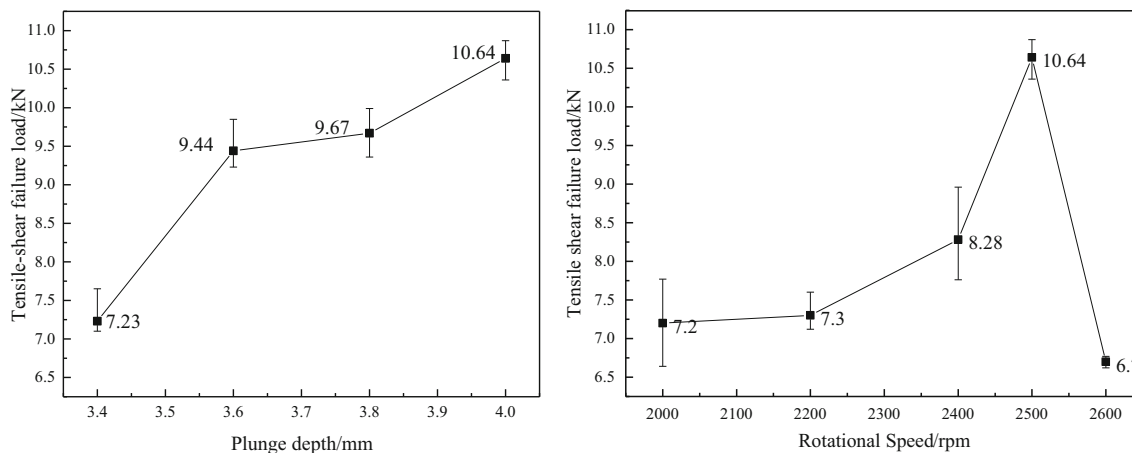
Fig. 9 Effects of **a** plunge depth and **b** rotation speed on mean tensile-shear load
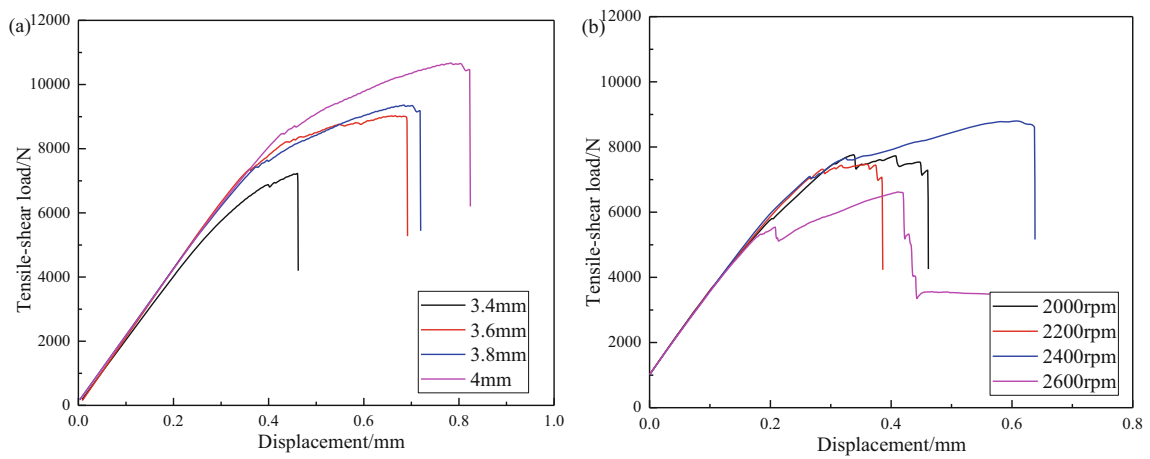
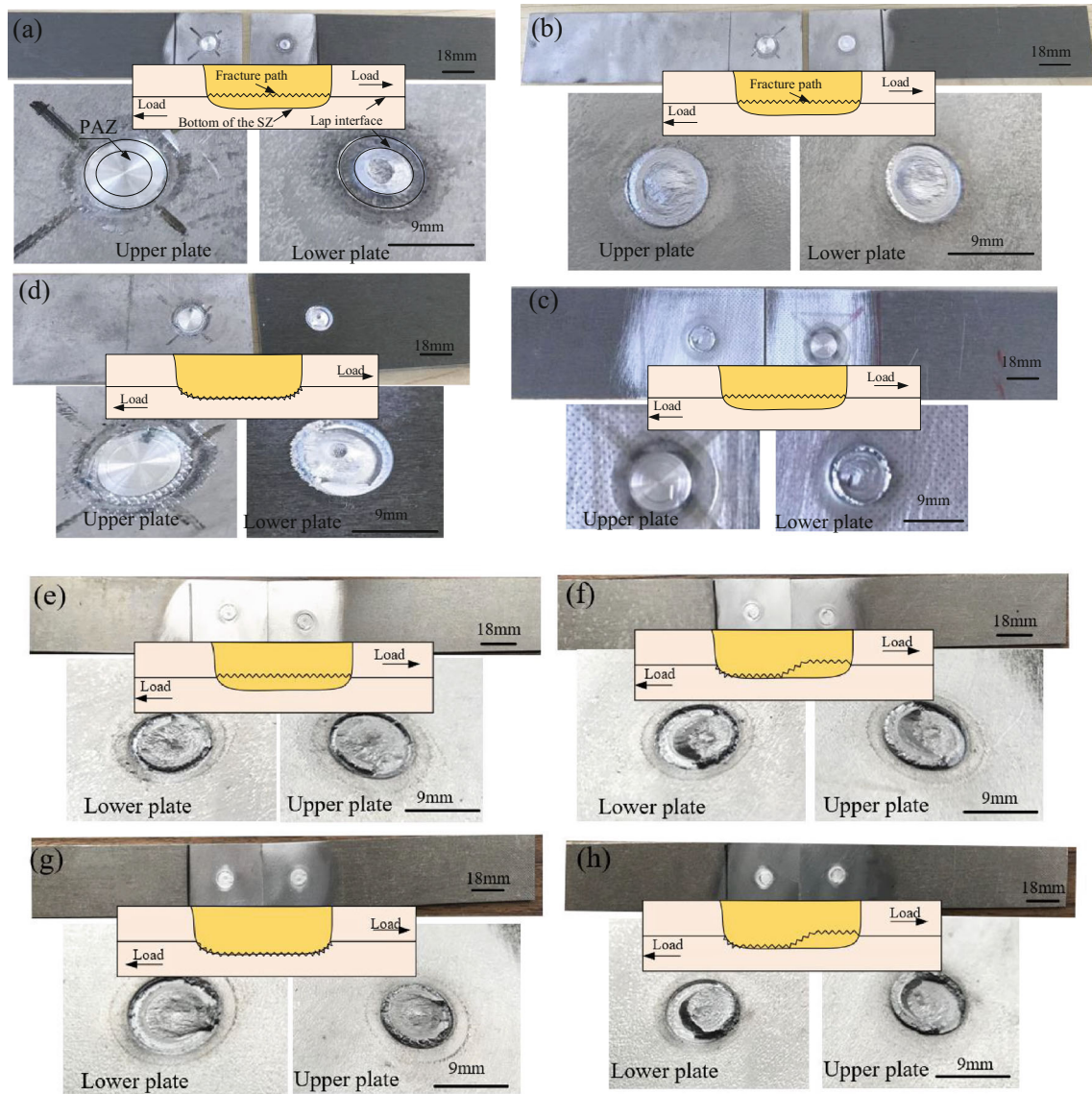Fig. 10 Load-displacement curves of refill FSSW joints at different **a** plunge depths and **b** rotation speeds

Fig. 11 Fracture paths of tensile-shear specimens of refill FSSW joints: under different plunge depths: **a** 3.4, **b** 3.6, **c** 3.8, and **d** 4 mm; under different rotation speeds: **e** 2000, **b** 2200, **c** 2400, and **d** 2600 rpm

Fig. 12 Fracture surface morphologies of tensile-shear specimens for refill FSSW joints: **a** under plunge depth of 3.4 and **b** 4 mm; **c, d** welding defects at the bottom of the SAZ
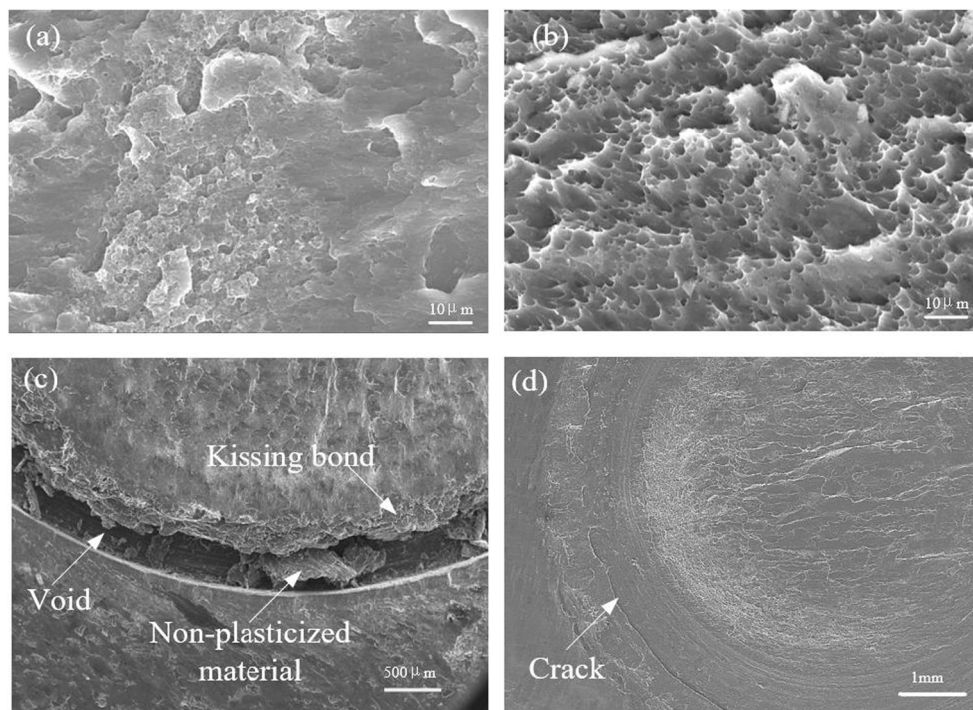
2500 rpm, the whole region at the bottom of the SZ of joint is sheared (Fig. 11 g and d). When the rotation speed continues to increase to 2600 rpm, tensile-shear specimens present the similar fracture path as that at the rotation speed of 2200 rpm (Fig. 11f and h).

Figures 12a and b show the magnified views of the region at the bottom of the PAZ for fracture specimens at different tensile-shear loads. The fracture surface of the tensile-shear specimen at the higher tensile-shear load consist of numerous shear dimples (Fig. 12b), and the size and quantity of the dimples are reduced when the tensile-shear load of the joint is small. Although the dimples are small, they also prove that the lap interface is welded. The different fracture surface morphologies present different bonding degree of lap interface. Figure 12c and d show fracture surface of the region at the bottom of the SAZ.

There exist obvious characteristics of welding defects such as void, kissing bond, and crack.

The welding defects influence crack initiation and propagation and then tensile-shear properties of refill FSSW joints. As mentioned above, the welding defects usually occur in the micro-junction region where plastic material is refilled. Furthermore, the fracture behavior of refill FSSW joint is closely related to the micro-junction structure.

4 Discussion

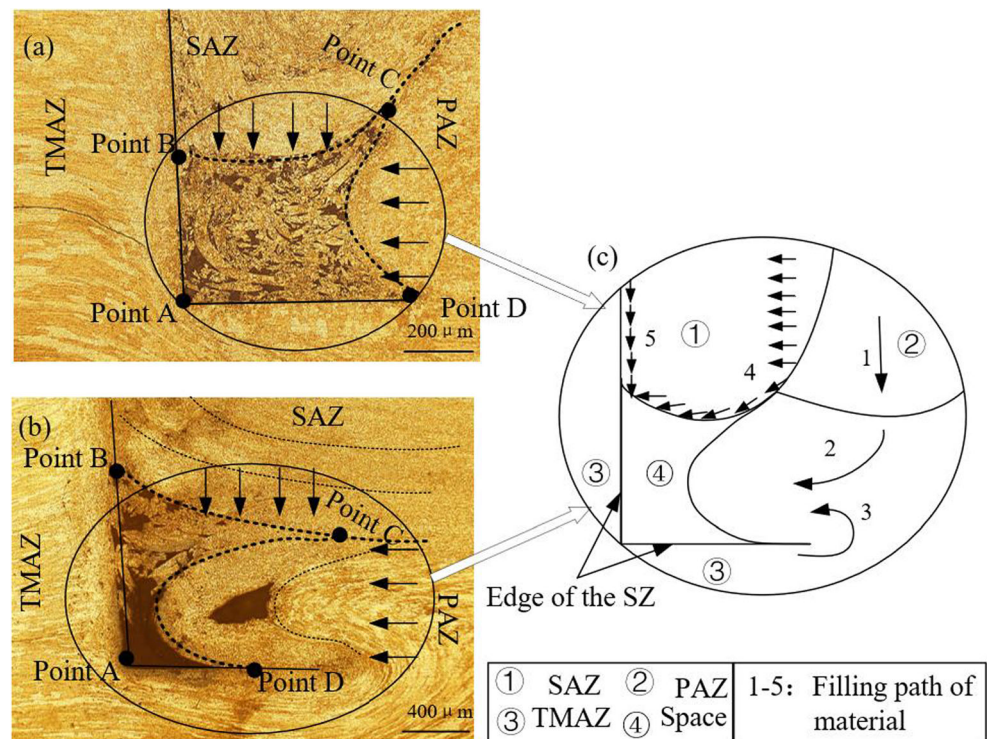### 4.1 Formation mechanism of micro-junction structure

Welding quality of the refill FSSW joint is closely related to the plastic material flow. Cao et al. [21] simulated the

Fig. 13 Schematic of division for cross section
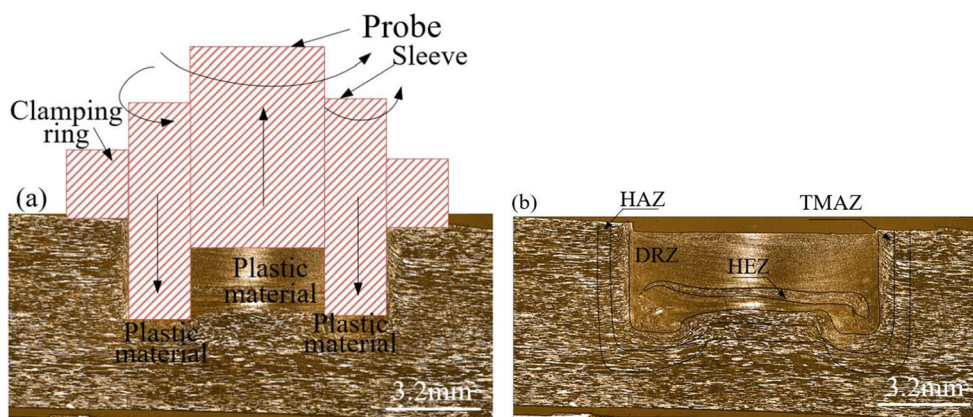
Fig. 14 Micro-junction structure inside the refill FSSW joint

distribution of SZ material at different times at plunging and refilling phases, and reported the material flow rules. Meanwhile, Cao et al. [21] revealed that the hook is associated with the inadequate material deformation and low material diffusion rate. Under different rotation speeds and dwell times, void and hook are both observed at different aluminum alloys refill FSSW joints, and Shen et al. [15, 16] pointed out the defects are related to the material flow due to improper welding parameters. Oliveria et al. [18] attributed the formation of void to thermal shrinkage, entrapped air, or some physical–chemical structural changes. The void reduces the structural integrity and facilitates crack initiation and propagation.

At the plunging phase, the sleeve plunges into the sheets, and the plastic material is restricted to the space formed by the sleeve, the probe, and adjacent cold metals (Fig. 13a). This part of the plastic material is regarded as SZ. When the sleeve plunges into the sheets, the metal sheets are subjected to a stamping effect and the plastic material is squeezed into the rotation sleeve. This metal material can be divided into two parts. One is close contact with the inwall of the rotation sleeve and the bottom of the rotation probe. The other is the material which is not in contact with the welding tool. The former consisting of refine equiaxed grains is referred to dynamic recrystallization zone (DRZ). The latter undergone heat conduction and extruded by the probe is referred to heat extrusion zone (HEZ). The lap interface below the probe occurs diffusion bonding during the whole welding process, and it is characterized by equiaxed grains which is also regarded as

DRZ. The HEZ is surrounded by the DRZ, and thus the SZ is divided into the HEZ and the DRZ (Fig. 13b).

The refilling phase is the critical step for joint formation. At the beginning of the refilling, the space is generated as soon as the sleeve moves upwards (region ④ in Fig. 14c). Meanwhile, the probe moves downwards, and the material below the probe is subjected to vertical force and occurs upsetting. Thus, this material is used to fill the region ④ along the direction 2. Due to the viscosity action, material in region ② synchronously drives its adjacent material in region ③ to refill the space ④ along the direction 3. The rotation sleeve drives the SZ material to move circumferentially along the direction 4, and the screw thread outside the wall of the sleeve drives the material to move downwards along the direction 5. From Fig. 14a and b, regions ① and ③ belong to the SAZ and TMAZ, respectively. Region ② belongs to PAZ, and includes the DRZ and HEZ according to the microstructure morphologies in Fig. 13. In conclusion, the plastic material in regions ①, ②, and ③ is used for filling space ④ at the same time.

The micro-junction structure is formed at the bonding boundary, as circled in Fig. 14a and b. A "r-shaped" structure is formed by the different material flow paths of filling regions, and the tips of the "r-shaped" structure create bonding defects. With the continuous squeezing by the probe, regions ①, ②, and ③ fill the space ④ in the form of the wavy lines, as shown in the dashed line in Fig. 14b. Due to the differences in thermophysical or flow performance of filling material, filling interface for each layer easily generates defects. Thus, this micro-junction structure mainly depends on the plastic

material flow which is closely related to the welding parameters. When the welding parameters are improper, welding defects are produced at the micro-junction structure.

4.2 Effect of plunge depth on micro-junction structure

The void in different sizes and quantity is observed at the tip of the "r-shaped" micro-junction structure under different plunge depths and the fixed rotation speed of 2500 rpm (Fig. 15a–d). The kissing bond, crack, and void can also be seen along the filling paths. Due to the small ratio of the length to width for kissing bond, the kissing bond is regarded as crack in the schematics of micro-junction structure formation (Fig. 15e–h).

The welding time is short at the relatively small plunge depth of 3.4 mm, and the material in the SZ occurs incomplete plasticization, which result in a large-area dispersed void and crack at the boundary between regions ② and ③ (Fig. 15e). With the continuous squeezing of the probe, the material in regions ③ and ⑤ comes into contact, and due to different thermophysical properties of material in regions ③ and ⑤, void and crack are generated at the bonding interface (Fig. 15a). Furthermore, the crack is also obvious in the filling paths in region ①.

As analyzed above, the heat input increases as the plunge depth increases from 3.4 to 3.8 mm, and then the material flow. Therefore, the region of the dispersed void at the bottom of the SAZ gradually reduces, and even only a small size void can be seen (Fig. 15b–c). Furthermore, the size and the number of the crack in the filling paths are also reduced with increasing plunge depth. However, the increase of the heat input leads to large difference in thermophysical properties of materials in region ③ and region ④ (Fig. 15f–g). Therefore, there still exists void at the bonding interfaces. Flow stress of thermoplastic materials reduces with the increased plunge depth, and much more thermoplastic material is used to fill region ④. At the same time, the kissing bond and void in the filling interface between regions ③ and ② are gradually decreased. When the plunge depth increases to 4 mm, there still exists void in the micro-junction structure, but the void is small and scattered (Fig. 15d).

In conclusion, the welding defects in the tip of the micro-junction structure gradually decrease with the increase of the plunge depth from 3.4 to 4 mm. Furthermore, the kissing bond, crack, and void at the bonding interface and filling path are decreased and even eliminated.

4.3 Effect of rotation speed on micro-junction structure

When the rotation speed is in the range of 2000–2600 rpm at the plunge depth of 4 mm, the void in different sizes (Fig. 16b–d) are observed in the micro-junction structure at the bottom of the SAZ.

At the fixed plunge depth, rotation speed is the critical factor to determine the welding quality of the refill FSSW joint. The space below the sleeve (region ④) is mainly refilled by the material in the SAZ (region ①), PAZ (regions ② and ⑤), and TMAZ (region ③) below the probe. The PAZ can be divided into material at the lap interface (region ⑤) and above the lap interface (region ②).

When the rotation speed is only 2000 rpm, the heat input is insufficient. The flow stress of thermoplastic material of the SZ and the viscosity of the material in the TMAZ driven by this SZ material are rather large. Thus, under the effect of the squeezing by the probe, the filling ability of material in regions ①, ②, ③, and ⑤ is weak, and the height of void at the micro-junction structure is large and measures 1407.90 μm (Fig. 16a).

When the rotation speed increases from 2000 to 2400 rpm, much more material is driven to refill the space ④ under the squeezing of the probe. At the rotation speed of 2200 rpm, the height of the dispersed void is reduced to 1355.26 μm (Fig. 16b). When the rotation speed increases to 2400 rpm, the plastic material flow becomes better, and the dispersed void is further reduced (Fig. 16c). The dispersed void is shrunk to void in small size at the rotation speed of 2500 rpm (Fig. 15d). However, the large-area dispersed void occurs again when the rotation speed increased to 2600 rpm (Fig. 16d), which may be related to the over-softened of material. The result is similar as that reported by Kubit et al. [22]. The scholar found that the increase of rotation speed or plunging time leads to an increase in the heat input of the welded materials. However, when the heat input exceeds a certain critical value, the welded sheets are overheated and then weakened [20]. In this study, under the high rotation speed of 2600 rpm, the metal material in regions ② and ⑤ may be over-softened and has small viscosity, which can be completely refilled to the region ④. However, the over-high temperature causes the material different from their adjacent material in temperature and microstructure. Thus, there still exists a large defect in the micro-junction structure when the rotation speed is higher a critical value.

Figures 16e–h shows the schematics of formation of micro-junction structure at different rotation speeds. Under the effect of squeezing of the probe, the material in regions ②, ③, and ⑤ is used to fill region ④. Meanwhile, under the effect of rotation sleeve and screw thread, material in region ① is also filled the region ④. Material in different regions has different filling modes, and the micro-junction structure is formed at the bottom of the SAZ. Due to different plasticized material at different rotation speeds, the void in different sizes is formed at this micro-junction structure.

4.4 Effect of micro-junction structure on fracture path

From the above analysis, there exist kissing bond, crack, and void in different sizes along the filling path and in the micro-
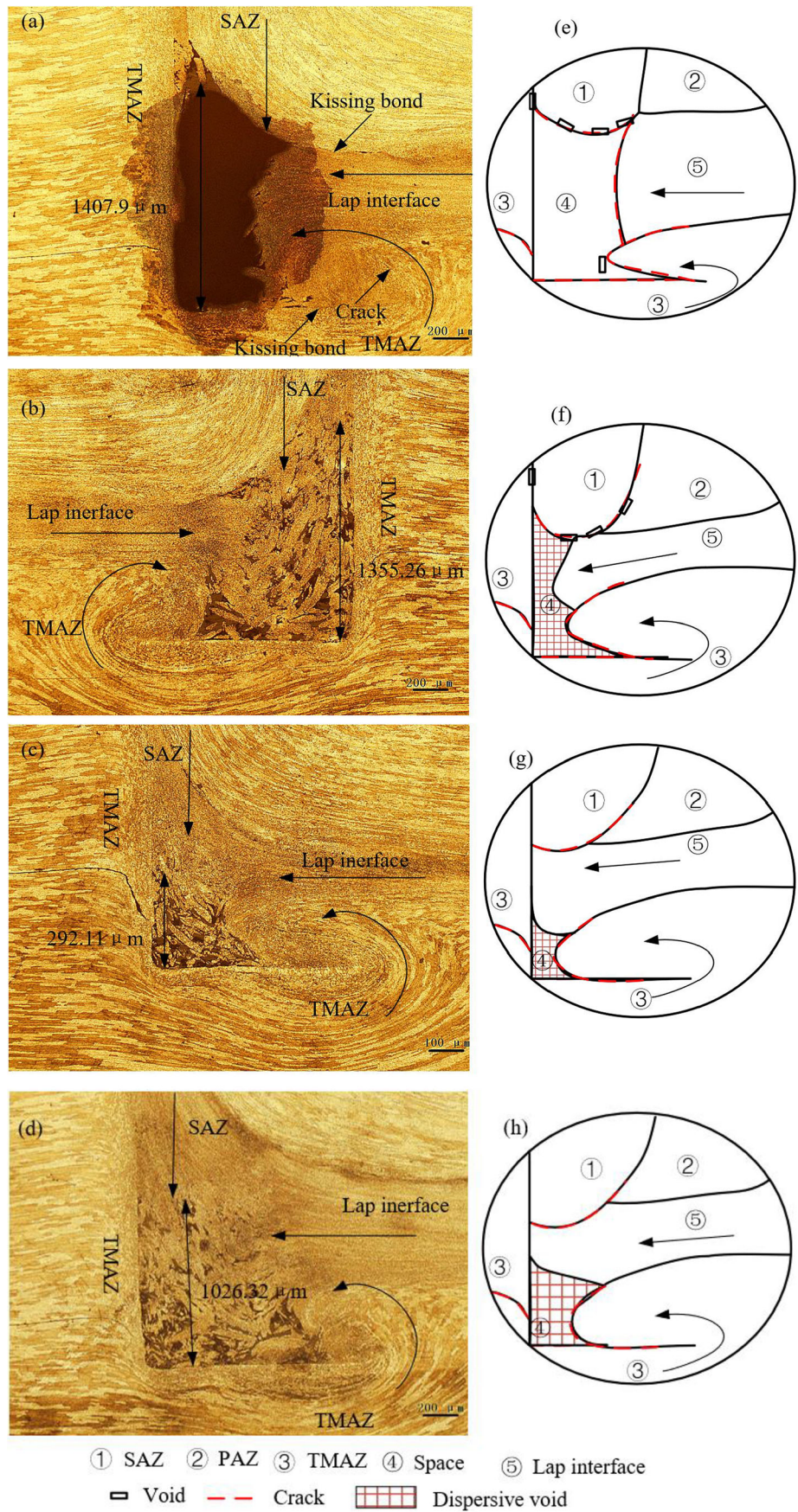
Fig. 15 Effect of plunge depth on the micro-junction structure: **a**, **e** 3.4 mm; **b, f** 3.6 mm; **c**, **g** 3.8 mm; **d**, **h** 4 mm
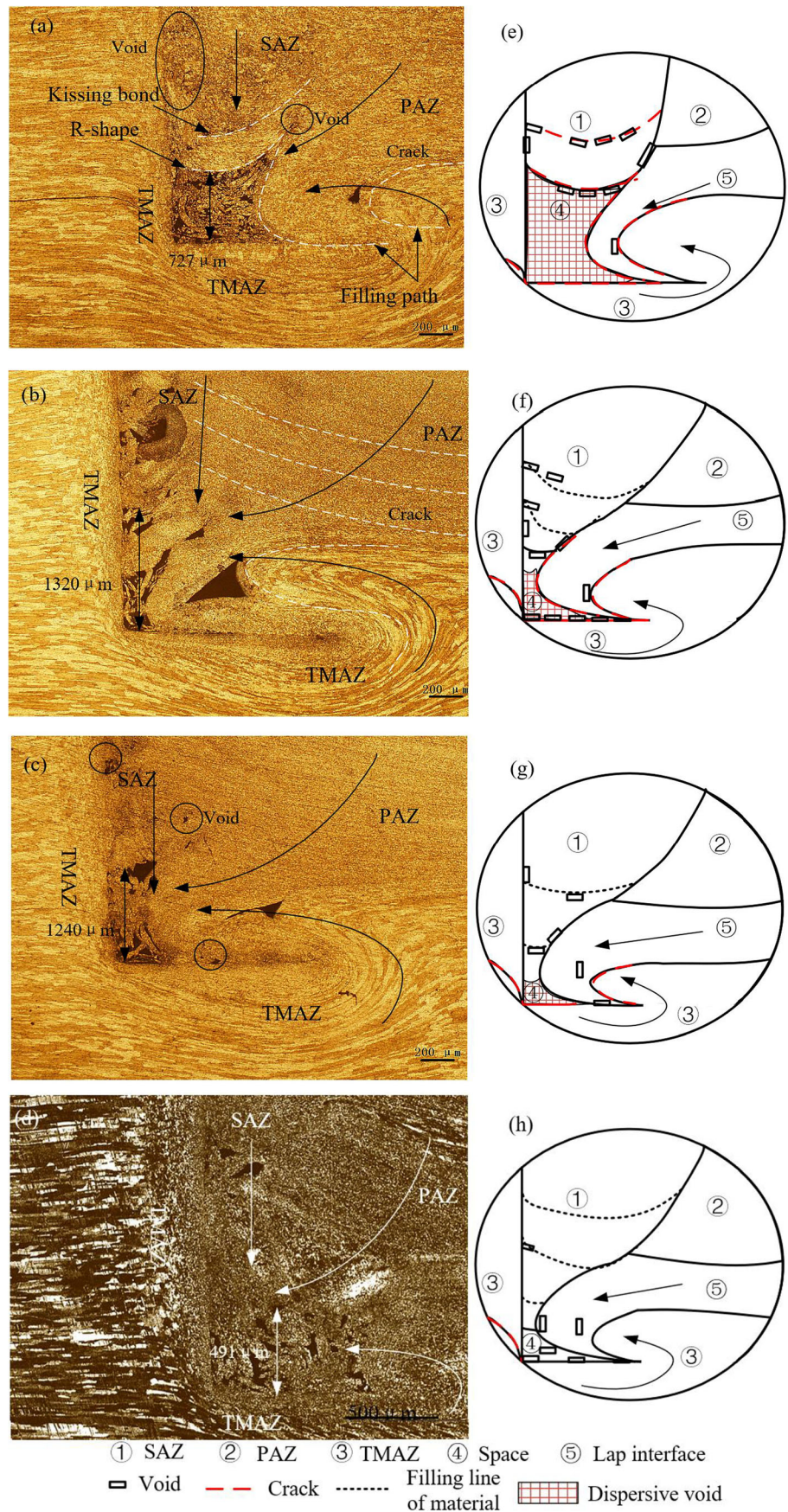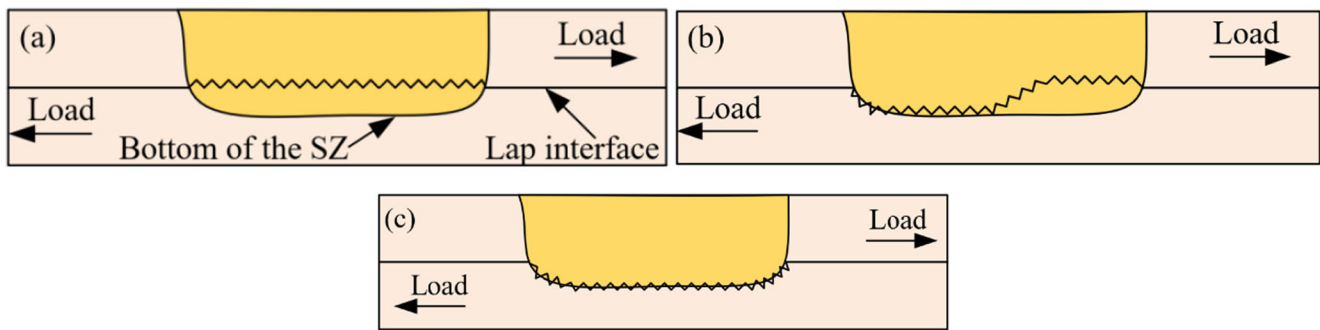
Fig. 16 Effect of rotation speed on the micro-junction structure: **a, e** 2000 rpm; **b, f** 2200 rpm; **c, g** 2400 rpm; **d, h** 2600 rpm

① SAZ　② PAZ　③ TMAZ　④ Space　⑤ Lap interface

▭ Void　‒ ‒ Crack　▦ Dispersive void

Fig. 17 Schematics of facture paths of tensile-shear specimens: **a** path I, **b** path II, and **c** path III
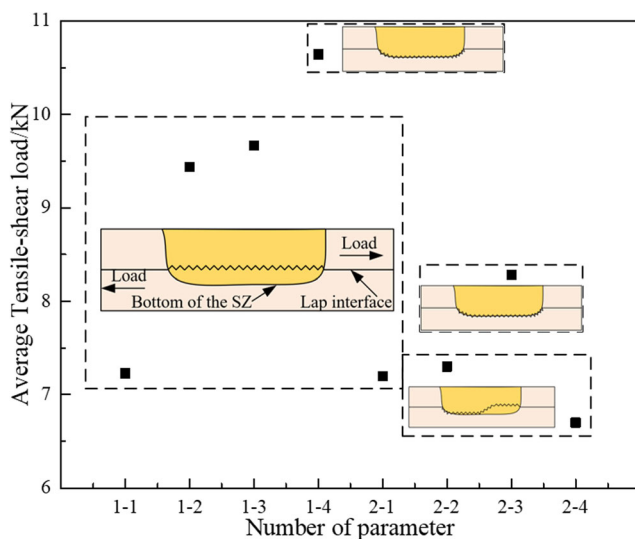
junction structure under different welding parameter combinations (Figs. 15–16). Under the external load, crack easily propagates into the bonding interface. For other series of aluminum alloys whose thickness is less than or equal to 2 mm, various fracture paths are obtained under different welding parameter combinations [19, 22, 23]. Li et al. [19] investigated the fracture mechanism of the 2024 aluminum alloy refill FSSW joint, and three different types of fracture modes are obtained, including shear fracture, shear-plug fracture, and plug fracture. Kubit et al. [22] and Zhou et al. [23] only obtained two of these three types of fracture modes for (1.6 + 0.8 mm) thick 7075-T6 aluminum alloy and (2 + 2 mm) thick 6061-T6 aluminum alloy RFSSW joints, respectively. In this study, only the shear fracture mode was observed for 3.2-mm-thick 2060 aluminum alloy refill FSSW joints. However, the investigation also found that the refill FSSW joints still have different fracture paths under the same fracture mode. Thus, this paper is concentrated on the shear fracture behavior in detail. From the analysis of the fracture path of refill FSSW joints (Fig. 11), it can be concluded that three different fracture paths can be obtained under different welding parameter combinations (Fig. 17). The lap interface fracture is referred to

path I. The fracture along the lap interface and the SZ bottom is referred to path II, and the fracture along the bottom of the SZ is referred to path III.

Figure 18 shows the mean tensile-shear load and fracture paths of refill FSSW joints. Sample numbers are the same as those in Table 1. The joints of 1-4 and 2-3 show the same fracture path, but their mechanical properties differ greatly. There is not an absolute relationship between fracture paths and tensile-shear loads of refill FSSW joints. The rotation speeds of 1-4 and 2-3 are 2500 and 2400 rpm at the fixed plunge depth of 4 mm, respectively. The same fracture paths of tensile-shear specimens under different welding parameter combinations indicate that the tensile-shear specimens have the same crack initiation sources and crack propagation paths. However, the number of the crack initiation sources and crack propagation resistance determine the fracture loads of tensile-shear specimens.

The cracks initiate at the welding defects in the micro-junction structure under the external load. The large-area dispersed void is generated at the joint under the rotation speed of 2400 rpm (Fig. 5c and g), which increases the crack initiation sources. When the rotation speed increases to 2500 rpm, the area of the dispersed void reduces (Fig. 4d and h) and then the crack initiation sources, which prove that the increase of the heat input facilitates the material flow in the micro-junction structures. Furthermore, the increase of the heat input also increases the bonding strength of the lap interface. Hence, although the same fracture paths are obtained at rotation speed of 2400 rpm and 2500 rpm, the fewer crack initiation sources inside the joint and the larger bonding strength of the lap interface at the rotation speed of 2500 rpm are beneficial to improving the tensile-shear properties.

During the tensile-shear tests, the sleeve-plunger interface and horizontal interface generate normal stress and shear stress, respectively. In this study, the welding defects at the bottom of the SAZ decrease the load-carrying area, and the effective bonding height is expressed as plunge depth minus the defect height. The previous results show that the normal stress is smaller than the shear stress of joint when the bonding height of the sleeve-plunger interface is lower than π mm for 3.2-mm-thick aluminum alloys [24]. Table 2 shows the values

Fig. 18 Mean tensile-shear load and fracture paths of tensile-shear specimens under different welding parameter combinations

Table 2 Bonding height of joints under different welding parameter combinations

| Number	1-1	1-2	1-3	1-4	2-1	2-2	2-3	2-4
Height of void/mm	0.727	1.320	1.240	0.491	1.408	1.355	0.292	1.026
Bonding height/h/mm	2.673	2.28	2.56	2.709	1.792	1.845	2.908	2.174

of bonding height of joints under different welding parameter combinations. Note that all the values of bonding height are lower than π mm. However, all the tensile-shear specimens present the shear fracture mode. The reason why the cracks propagate along the horizontal interface can be explained by the different bonding strength between the sleeve-plunger interface and horizontal interface, which has been expounded by the previous research [24].

The stress concentration is generally produced at the tip of the bending hook (point A, as shown in Figs. 19a–21a) under the external load. The cracks propagate along the direction with the lowest resistance at the micro-junction structure where filling material at different regions converges. For the joints at the small plunge depth or the low rotation speed, the insufficient heat input causes the incomplete bonding of the lap interface (Fig. 7), and the incomplete bonding is similar as cracks at the lap interface. Meanwhile, the upper and lower materials adjacent to the lap interface present different morphologies (Figs. 7 and 8a). Thus, the load-carrying capacity of the region at the bottom of the SZ is larger than the lap interface, and then the cracks propagate into the lap interface

(towards point B) with increasing external load (Fig. 19b). Finally, the tensile-shear specimens fracture along the lap interface (Fig. 19c).

Much more metal material is squeezed into the sleeve for the joints under the plunge depth of 4 mm compared with the joints below 4 mm, and this metal material has different plasticized conditions under different rotation speeds. When the rotation speed is only 2000 rpm, the inadequate heat input makes the lap interface low bonding strength. Due to the large area welding defects and discrepant microstructures at the lap interface (Fig. 8a), the tensile-shear specimens still fracture along the lap interface at 2000 rpm. When the rotation speed increases to 2200 rpm, the heat input increases the diffusion capacity of atoms at the lap interface. The anti-shear ability of the lap interface is even equal to the region at the bottom of the SZ. Furthermore, the equiaxed grains at the lap interface are located between the squeezed grains and elongated grains (Fig. 8b). Therefore, under the external load the lap interface and the region at the bottom of the SZ bear synchronously the shear stress. The crack of point A extends into point B, and the crack of point A′ propagates into the lap interface (Fig. 20b).

Fig. 19 Fracture processes of path I: **a** crack initiation, **b** crack propagation, and **c** fracture
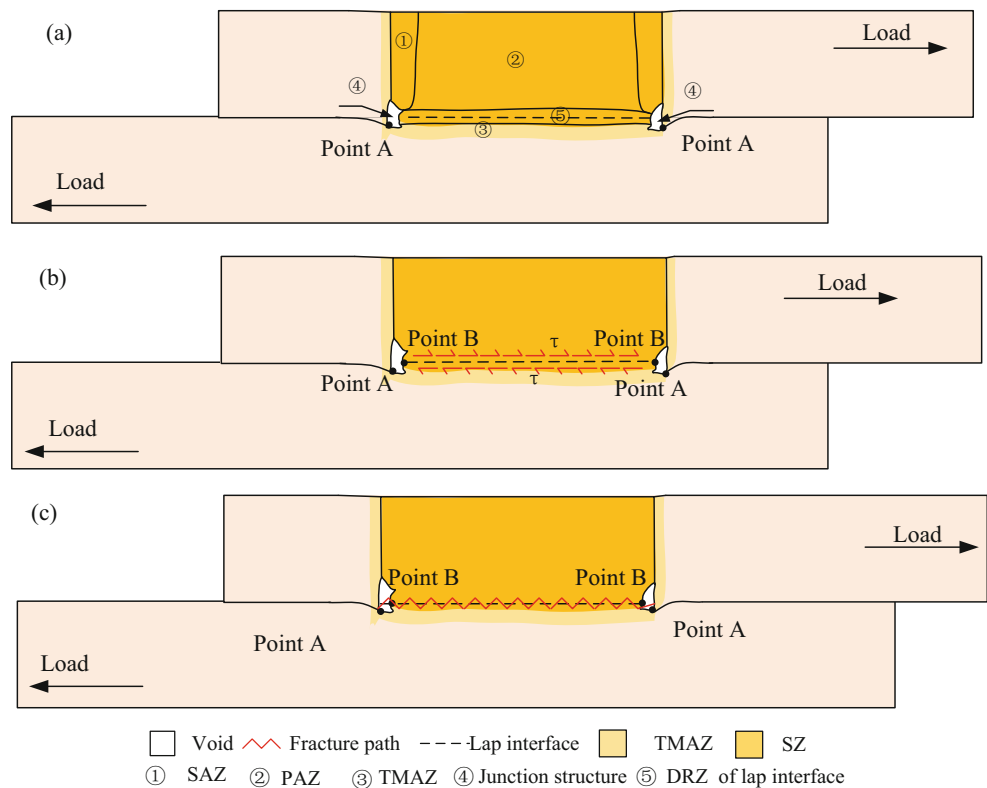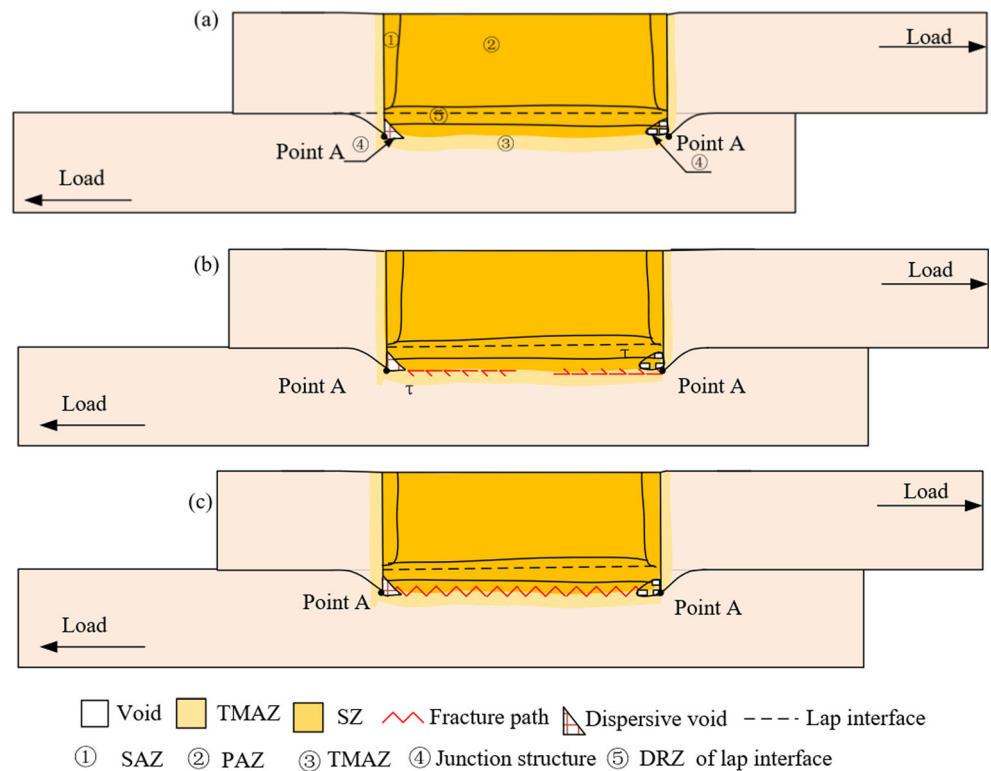
Fig. 20 Fracture processes of path II: **a** crack initiation, **b** crack propagation, and **c** fracture
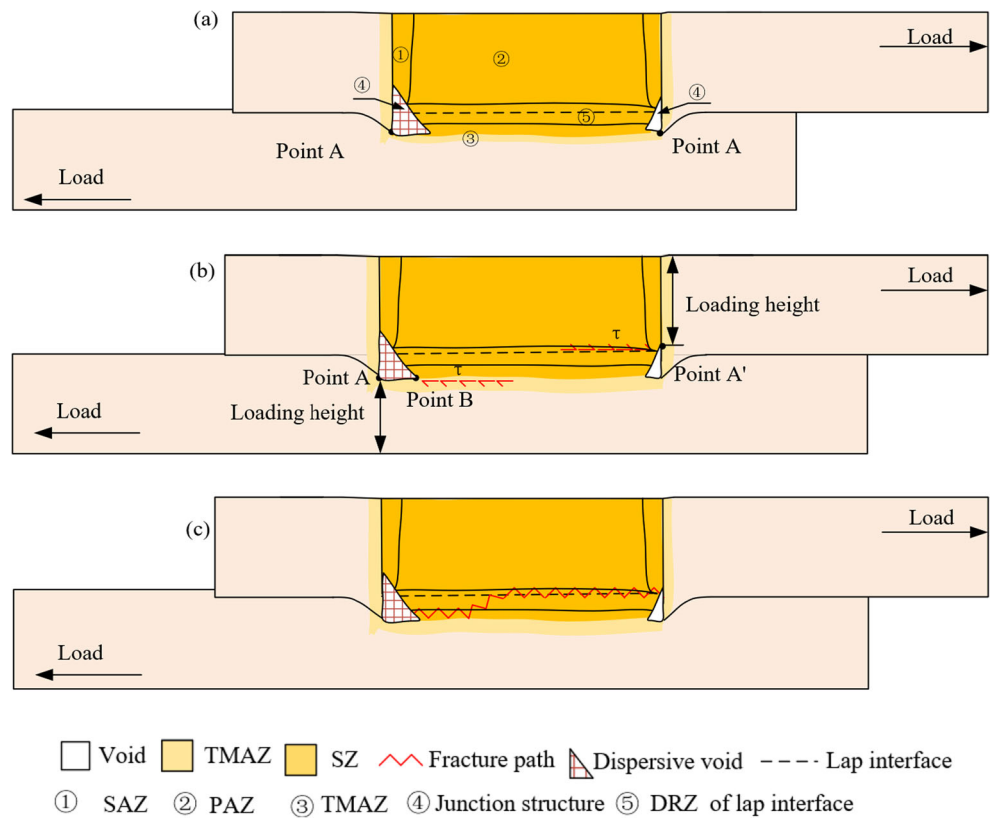
With the continuous propagation of cracks to the interior of the welding spot, the fracture surface of the junction region is in the direction of 45° with tensile-shear load (Fig. 20c).

Fig. 21 Fracture processes of path III: **a** crack initiation, **b** crack propagation, and **c** fracture

The heat input continues to increase when the rotation speed increases to 2400 and 2500 rpm under the fixed plunge depth of 4 mm. Consequently, the bonding strength of the lap interface also increases, and even is higher than that of the region at the bottom of the SZ. Meanwhile, the anti-shear ability of the region at the bottom of the SZ is lower than that at the lap interface. Moreover, the thickness of the lap interface with refined and equiaxed grains is widened (Figs. 7d and 8c), which also increases the ability of resistance to deformation. The shear stress is mainly shared by the region at the bottom of the SZ (Fig. 21b). When the tensile-shear load of joint exceeds the ultimate load of joint, the tensile-shear specimens fracture along the bottom of the SZ (Fig. 21c).

In conclusion, there exist three fracture paths for the tensile-shear specimens of 3.2-mm-thick aluminum alloys under different plunge depths and rotation speeds. The fracture location is related to the welding defects and the anti-shear ability of horizontal interface.

From the abovementioned results and discussion, it can be concluded that the welding defects in the micro-junction structure have important influences on the tensile-shear properties. The formation of these defects is associated with the adequately unplasticized material and the delayed filling of material. Thus, from the viewpoint of obtaining the defect-free welding joint with higher tensile-shear load, further increasing the heat input or refilling speed within a reasonable range is an effective approach to optimize the welding parameters.

5 Conclusion

The refill FSSW experiments for 3.2-mm-thick 2060 aluminum alloys were conducted at different plunge depths and rotation speeds. The formation mechanism of micro-junction structure and effects of welding parameters on the micro-junction structure and fracture behavior of refill FSSW joints were analyzed. The conclusions are as follows.

1. Different filling modes of material in the TMAZ, PAZ, and SAZ cause the "r-shape" micro-junction structure at the bottom of the SAZ. The plasticized degree of filling material and refilling time greatly influence the morphologies of micro-junction structure.
2. The welding defects such as voids with different sizes, crack, and kissing bond are easily formed in the micro-junction structure. These defects are reduced as the plunge depth increases from 3.4 to 4 mm at the fixed rotation speed of 2500 rpm. The large-area dispersed voids are reduced as the rotation speed increases from 2000 to 2500 rpm at the plunge depth of 4 mm.
3. The tensile-shear load of the refill FSSW joint gradually increases with increasing plunge depth from 3.4 to 4 mm, and firstly increases and then decreases as the rotation speed increases from 2000 to 2600 rpm. The maximum tensile-shear load of 10.64 kN is obtained when the plunge depth of 4 mm and the rotation speed of 2500 rpm are used.
4. Three failure paths are obtained: first, along the lap interface; second, along the SAZ bottom; and third, along both of them. The micro-junction structure and the bonding strength of the lap interface are the main factors to influence tensile-shear load and the fracture behavior.

Authors' contributions All authors contributed to the study conception and design. Material preparation, data collection, and analysis were performed by Yue Wang and Peng Chai. The first draft of the manuscript was written by Yue Wang and all authors commented on previous versions of the manuscript. All authors read and approved the final manuscript.

Compliance with ethical standards

Conflict of interest The authors declare that they have no conflict of interest.

References

1. Chu Q, Li WY, Yang XW, Shen JJ, Li YB, Wang WB (2017) Study of process/structure/property relationships in probeless friction stir spot welded AA2198 Al-Li alloy. Weld World 61(2):291–298
2. Beaudoin AJ, Obstalecki M, Tayon W, Hernquist M, Mudrock R, Kenesei P, Lienert U (2013) In situ assessment of lattice strain in an Al-Li alloy. Acta Mater 61:3456–3464
3. Santana LM, Suhuddin UFH, Ölscher MH, Strohaecker TR, Santos JFD (2017) Process optimization and microstructure analysis in refill friction stir spot welding of 3-mm-thick Al-Mg-Si aluminum alloy. Int J Adv Manuf Tech 92:4213–4220
4. Vijayakumar P, Madhusudhanreddy G, Srinivasarao K (2015) Microstructure, mechanical and corrosion behavior of high strength AA7075 aluminium alloy friction stir welds-effect of post weld heat treatment. Def Technol 11:362–369
5. Lacki P, Derlatka A (2016) Experimental and numerical investigation of aluminium lap joints made by RFSSW. Meccanica 51:455–462
6. Chai P, Wang Y (2019) Effect of rotational speed on microstructure and mechanical properties of 2060 aluminum alloy RFSSW joint. Met Mater Int 25:1574–1585
7. Caroline DCC, Henrique PA, Guedes DAN, Fernandes DSJ (2018) Taguchi approach for the optimization of refill friction stir spot welding parameters for AA2198-T8 aluminum alloy. Int J Adv Manuf Tech 99:1927–1936
8. Tier MD, Rosendo TS, Santos JFD, Huber N, Strohaecker TR (2013) The influence of refill FSSW parameters on the microstructure and shear strength of 5042 aluminium welds. J Mater Process Tech 213:997–1005
9. Kluz R, Kubit A, Trzepiecinski T, Faes K (2019) Polyoptimisation of the refill friction stir spot welding parameters applied in joining

7075-t6 Alclad aluminium alloy sheets used in aircraft components. Int J Adv Manuf Tech 103:3443–3457

10. Adamus J, Adamus K (2019) The analysis of reasons for defects formation in aluminum joints created using RFSSW technology. Manuf lett 21:35–40

11. Zhao YQ, Liu HJ, Chen SX, Lin Z, Hou JC (2014) Effects of sleeve plunge depth on microstructures and mechanical properties of friction spot welded alclad 7B04-T74 aluminum alloy. Mater Des 62: 40–46

12. Yang XW, Fu T, Li WY (2014) Friction stir spot welding: a review on joint macroand microstructure, property, and process modelling. Adv Mater Sci Eng 1:1–11

13. Wang Y, Chai P, Ma H, Cao XM, Zhang YH (2020) Formation mechanism and fracture behavior in extra-filling refill friction stir spot weld for Al-Cu-Mg aluminum alloy. J Mater Sci 55:358–374

14. Yue YM, Shi Y, Ji SD, Zhang LG, Wang Y (2017) Effect of sleeve plunge depth on microstructure and mechanical properties of refill friction stir spot welding of 2198 aluminum alloy. J Mater Eng Perform 26:5064–5071

15. Shen ZK, Yang XQ, Zhang ZH, Cui L, Li TL (2013) Microstructure and failure mechanisms of refill friction stir spot welded 7075-T6 aluminum alloy joints. Mater Des 44:476–486

16. Shen ZK, Yang XQ, Yang S, Zhang ZH, Yin YH (2014) Microstructure and mechanical properties of friction spot welded 6061-T4 aluminum alloy. Mater Des 54:766–778

17. Shi Y, Yue YM, Zhang LG, Wang Y (2017) Refill friction stir welding of 2198-T8 aluminum alloy. T Indian I Metals 71:139–145

18. Oliveira PHF, Amancio-Filho ST, Dos Santos JF, Hage E Jr (2010) Preliminary study on the feasibility of friction spot welding in PMMA. Mater Lett 64:2098–2101

19. Li ZW, Ji SD, Ma YN, Chai P, Yue YM, Gao SS (2016) Fracture mechanism of refill friction stir spot-welded 2024-T4 aluminum alloy. Int J Adv Manuf Technol 86:1925–1932

20. Zhao YQ, Wang CG, Dong CL, Deng J, Tan JH (2018) Numerical study on a thermal process in friction spot welding of Al-Zn-Mg-Cu alloy. Weld World 62:931–939

21. Cao JY, Wang M, Kong L, Yin YH, Guo LJ (2017) Numerical modeling and experimental investigation of 798 material flow in friction spot welding of Al 6061-T6. Int J Adv Manuf Technol 89: 2129–2139

22. Kubit A, Bucior M, Wydrzyński D, Trzepieciński T, Pytel M (2018) Failure mechanisms of refill friction stir spot welded 7075-T6 aluminium alloy single-lap joints. Int J Adv Manuf Technol 94: 4479–4491

23. Zhou L, Luo LY, Zhang TP, He WX, Feng JC (2017) Effect of rotation speed on microstructure and mechanical properties of refill friction stir spot welded 6061-T6 aluminum alloy. Int J Adv Manuf Technol 92:3425–3433

24. Wang Y, Chai P. Characteristics and tensile-shear properties of refill FSSW joint under different plunge depths in 2060 aluminum alloy. Archives of Metallurgy and Materials, Accept

Ⓐ Springer